ADVANCED MATERIALS
www.advmat.de

Defect-Engineering-Enabled High-Efficiency All-Inorganic Perovskite Solar Cells

*Jia Liang, Xiao Han, Ji-Hui Yang, Boyu Zhang, Qiyi Fang, Jing Zhang, Qing Ai, Meredith M. Ogle, Tanguy Terlier, Angel A. Martí, and Jun Lou**

The emergence of cesium lead iodide ($CsPbI_3$) perovskite solar cells (PSCs) has generated enormous interest in the photovoltaic research community. However, in general they exhibit low power conversion efficiencies (PCEs) because of the existence of defects. A new all-inorganic perovskite material, $CsPbI_3$:Br:InI_3, is prepared by defect engineering of $CsPbI_3$. This new perovskite retains the same bandgap as $CsPbI_3$, while the intrinsic defect concentration is largely suppressed. Moreover, it can be prepared in an extremely high humidity atmosphere and thus a glovebox is not required. By completely eliminating the labile and expensive components in traditional PSCs, the all-inorganic PSCs based on $CsPbI_3$:Br:InI_3 and carbon electrode exhibit PCE and open-circuit voltage as high as 12.04% and 1.20 V, respectively. More importantly, they demonstrate excellent stability in air for more than two months, while those based on $CsPbI_3$ can survive only a few days in air. The progress reported represents a major leap for all-inorganic PSCs and paves the way for their further exploration in order to achieve higher performance.

Dr. J. Liang, Dr. X. Han, B. Zhang, Q. Fang, Dr. J. Zhang, Q. Ai, Prof. A. A. Martí, Prof. J. Lou
Department of Materials Science and NanoEngineering
Rice University
Houston, TX 77005, USA
E-mail: jlou@rice.edu

Dr. J. Liang, Prof. A. A. Martí, Prof. J. Lou
Smalley-Curl Institute
Rice University
Houston, TX 77005, USA

Dr. X. Han
School of Materials Science and Engineering
Northwestern Polytechnical University
Xi'an 710072, China

Dr. J.-H. Yang
Department of Physics
Fudan University
Shanghai 200433, China

M. M. Ogle, Prof. A. A. Martí, Prof. J. Lou
Department of Chemistry
Rice University
Houston, TX 77005, USA

Dr. T. Terlier
Shared Equipment Authority
SIMS laboratory
Rice University
Houston, TX 77005, USA

The ORCID identification number(s) for the author(s) of this article can be found under https://doi.org/10.1002/adma.201903448.

DOI: 10.1002/adma.201903448

Hybrid organic–inorganic halide perovskite solar cells (PSCs) are considered as a promising photovoltaic technology for solar energy conversion owing to the remarkable increase of the power conversion efficiencies (PCEs) in the past few years.[1–5] These PSCs typically used the organic–inorganic perovskites comprising organic cations, such as methylammonium (MA) and formamidinium (FA), in a lead halide framework as the absorbers, giving the PCE exceeding 24%.[6–8] However, such organic cations suffer from poor photochemical and thermal stability issues.[9,10] Replacing the organic cations with inorganic cations (such as cesium) has been found to be effective to improve the stability.[11,12]

Inorganic cesium lead halide perovskites ($CsPbX_3$, X = I, Br, or mixture) thus have gained widespread attention due to their improved thermal stabilities and competitive optoelectronic properties as compared to the organic–inorganic halide perovskites.[13,14] Among these materials, $CsPbI_3$ is believed to be the most suitable active layer for PSCs because of its appropriate bandgap.[15] However, the cubic phase $CsPbI_3$ is not stable and quickly degrades to a yellow nonperovskite phase at room temperature, which basically does not absorb much sun light.[15] Till now, several efforts have been proposed to stabilize the cubic phase $CsPbI_3$ to fabricate efficient PSCs, such as reducing the crystal size to quantum dots, introducing an intermediate phase (e.g., Cs_4PbI_6), partially substituting the iodide with bromide or chloride, and others.[16–18] All these attempts showed enhanced performances yet still far from reaching the theoretical limits. Based on previous literature (Table S1, Supporting Information), although the cubic phase $CsPbI_3$ possesses a bandgap of 1.73 eV, most $CsPbI_3$ based PSCs displayed a low open-voltage (V_{OC}) of less than 1.0 V, which is most likely due to the unavoidable shallow- or deep-level defects formed in $CsPbI_3$ film during crystal formation.[19–35] It is well known that defects in perovskites, especially point defects, played an important role on determining the electron-hole pair diffusion length and V_{OC} of the PSCs. Deep-level defects were usually considered as the Shockley–Read–Hall nonradiative recombination centers and led to charge trapping and scattering, and finally inevitably resulted in inferior device performances and long-term instability issues. Therefore, it is imperative to rationally design novel all-inorganic perovskites with not only good stability but also less intrinsic defects.

Herein, based on cubic $CsPbI_3$, we developed a novel all-inorganic perovskite through a simple solution-phase process in ambient environment without the need of a glove box. Retaining the bandgap of $CsPbI_3$, this new perovskite possessed substantially decreased defects, as well as excellent stability under ambient condition. Moreover, to reduce the cost of the PSCs, we also replaced the expensive and labile organic hole transport layer and noble metal electrode by a carbon electrode. As a result, the all-inorganic PSCs with layered configurations of fluorine doped tin oxide (FTO)/compact TiO_2 (c-TiO_2)/mesoporous TiO_2 (m-TiO_2)/$CsPbI_3$:Br:InI_3/carbon exhibited a large V_{OC} of 1.20 V and a remarkable PCE of 12.04%. Additionally, these all-inorganic PSCs exhibited excellent stability under environment stress for more than two months.

To quantitatively estimate the nature and density of defects in $CsPbI_3$, we investigated native defects in $CsPbI_3$ using the density functional theory (DFT) calculation. $CsPbI_3$ has 12 native point defects: the vacancies V_{Cs}, V_{Pb}, and V_I; the interstitials Cs_i, Pb_i, and I_i; and antisite occupations Cs_{Pb}, Cs_I, Pb_{Cs}, Pb_I, I_{Cs}, and I_{Pb}, as shown in Figure S1 in the Supporting Information. The formation energy $\Delta H_f(\alpha, q)$ of a point defect α is a function of both the electron Fermi energy E_F and the chemical potential μ_i of the species involved in the defects

$$\Delta H_f(\alpha,q) = E(\alpha,q) - E(\text{perfect}) + \Sigma n_i\mu_i + q\left[E_F + \varepsilon_{VBM}(\text{perfect})\right] \quad (1)$$

where $E(\alpha, q)$ is the total energy of a supercell with defect α in the charge state q, E(perfect) is the total energy of the supercell without any defects; n_i is the number of atoms changed from the supercell; q is the number of electrons exchanged between the supercell and the corresponding thermodynamic reservoir in forming the defect; E_F is the Fermi energy referenced to the energy of the VBM (ε_{VBM}(perfect)). To satisfy Equation (1), the formation of $CsPbI_3$ can be realized in the blue region defined by lines connecting A, B, C, and D points, as shown in the chemical potential chart of Pb versus Cs (Figure S2, Supporting Information). It is obvious that $CsPbI_3$ is difficult to grow and the formation highly depends on the concentration of the Cs species. In order to calculate the $\Delta H_f(\alpha, q)$ of 12 native point defects, two chemical potential conditions are considered here at B (Pb-rich) and D (Pb-poor) points. **Figure 1**a,b gives the variation of the $\Delta H_f(\alpha, q)$ along with the corresponding E_F at B and D points, respectively. Under the Pb-rich condition, V_{Pb} has the lowest formation energy among all acceptor defects, and I_i has the lowest formation energy among all donor defects. Moreover, the Fermi level is pinned at 0.05 eV above the VBM by V_{Pb} and I_i. While under the Pb-poor condition, I_i and V_I possess the lowest formation energies among all donor and acceptor defects, respectively. In this case, the Fermi level is pinned at 0.75 eV above VBM by I_i and V_I. Therefore, a very low V_{OC} of 0.7 V should be obtained from the $CsPbI_3$ perovskites, which can be ascribed to a large number of defects produced by the elements of Pb and I (V_{Pb}, V_I, and I_i).

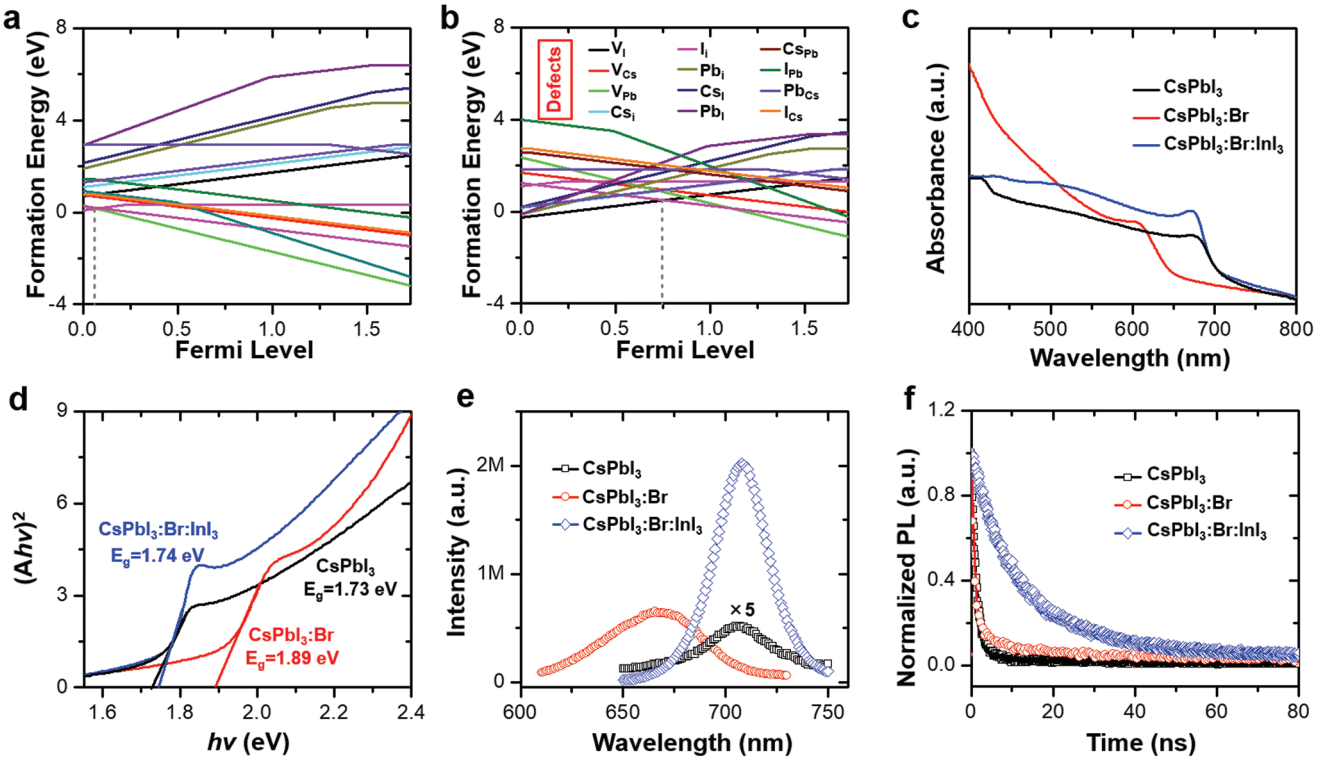

Figure 1. Defect formation energies of $CsPbI_3$ and photophysical properties of $CsPbI_3$, $CsPbI_3$:Br, and $CsPbI_3$:Br:InI_3 films. The defect formation energies as a function of Fermi level between the valence band maximum (VBM) and conduction band minimum (CBM) of native point defects in $CsPbI_3$ calculated under a) lead-rich and b) lead-poor growth condition. c) UV–vis absorption spectra, d) $(Ah\nu)^{[2]}$ versus $h\nu$ curves, e) PL spectra, and f) time-resolved PL decay of $CsPbI_3$, $CsPbI_3$:Br, and $CsPbI_3$:Br:InI_3 films, respectively. "×5" in inset (e) represents the data was expanded to the original by five times.

Since composition design has been known to be one of promising and facile methods for engineering defects, we partially replaced I^- and Pb^{2+} with Br^- and In^{3+}, respectively, and discovered that Br^- and In^{3+} played critical roles in controlling the defects. First, I^- ions were partially substituted by Br^- ions to suppress defects associated with the element of I. The performances of PSCs based on mixed-halide perovskites were improved; however, the compositional change leads to an undesirable increase in the bandgap. Subsequently, InI_3 was introduced into the precursors to partially replace PbI_2. Intriguingly, this material not only suppressed the related defects associated with Pb species, but also reduced the bandgap to the initial value of $CsPbI_3$. Hereafter, we labeled the material after introducing Br^- as $CsPbI_3$:Br, and the material after further introducing InI_3 as $CsPbI_3$:Br:InI_3. In this work, like previous literature, we used the feed ratio of precursors to clarify the exact composition of these samples.[36–38] For $CsPbI_3$:Br, I:Br = 1:2 was chose to guarantee the good stability. For $CsPbI_3$:Br:InI_3, Pb:In = 85:15 was used because the corresponding perovskite exhibited the smallest bandgap (Figure S3, Supporting Information).

Figure 1c shows the UV–vis absorption spectra of the $CsPbI_3$, $CsPbI_3$:Br, and $CsPbI_3$:Br:InI_3 films. When Br^- ions were incorporated, a blue shift is observed in the $CsPbI_3$:Br films. This can be ascribed to the large bandgap of 2.3 eV for $CsPbBr_3$. When InI_3 were further incorporated, a red shift is observed in the $CsPbI_3$:Br:InI_3 film. Moreover, we calculated the absorbance coefficients of $CsPbI_3$ and $CsPbI_3$:Br:InI_3 films from the measured optical transmittance and reflectance spectra according to the following equation: $\alpha = [\ln((1-R)/T)]/d$, where T, R, and d are the optical transmittance, reflectance, thickness of the films, respectively.[39] Figure S4 in the Supporting Information gives the curves of the absorption coefficient, averaged from the 400–700 nm wavelength range where no absorption band occurs, along with the thickness of these two kinds of films. Clearly, the $CsPbI_3$:Br:InI_3 film exhibits higher absorption coefficient than the $CsPbI_3$ film. Figure 1d displays the transformed plots from the UV–vis absorption spectra.[40–43] Bandgaps of $CsPbI_3$, $CsPbI_3$:Br, and $CsPbI_3$:Br:InI_3 films are determined to be 1.73, 1.89, and 1.74 eV, respectively. The $CsPbI_3$:Br:InI_3 film has the similar bandgap with the $CsPbI_3$ film, which suggests that the $CsPbI_3$:Br:InI_3 is also an appropriate absorber material in PSCs, especially for the tandem cells combining with silicon solar cells. In order to get a direct visual observation of such bandgap changes by naked eyes, digital pictures of $CsPbI_3$, $CsPbI_3$:Br, and $CsPbI_3$:Br:InI_3 films deposited on FTO/compact TiO_2 (c-TiO_2)/mesoporous TiO_2 (m-TiO_2) substrates were taken, as shown in Figure S5 in the Supporting Information. It clearly showed the same trend as observed in Figure 1c,d. Figure 1e shows the photoluminescence (PL) spectra of these samples, exhibiting a sharp emission peak around 707, 665, and 708 nm, for $CsPbI_3$, $CsPbI_3$:Br, and $CsPbI_3$:Br:InI_3 respectively, which is in consistent with the bandgaps obtained from Figure 1d. Moreover, Figure 1e also reveals that the PL intensity of the $CsPbI_3$:Br film is higher than that of the $CsPbI_3$ film, and the $CsPbI_3$:Br:InI_3 film has the highest PL intensity. This is consistent with the lowest defect density in the $CsPbI_3$:Br:InI_3 film. Therefore, a significantly reduced nonradiative recombination loss and improved photocurrent collection in these films can be expected after introducing Br^- and In^{3+} in the $CsPbI_3$ film. Figure 1f depicts the time-resolved PL (TRPL) decays of $CsPbI_3$, $CsPbI_3$:Br, and $CsPbI_3$:Br:InI_3 films. The corresponding PL lifetimes were calculated by biexponential fits to the TRPL decays. The fast decay lifetime (t_1) originates from the quenching of the photogenerated free carriers and the slow decay lifetime (t_2) is attributed to the radiative recombination of free carriers.[44] Clearly, after introducing Br^- and In^{3+} in the $CsPbI_3$ film, the $CsPbI_3$:Br:InI_3 film shows the longest lifetimes for both t_1 and t_2. Specifically, t_1 is 7.2 and t_2 is 18.1 ns, meanwhile their corresponding weight fractions are 29.76% and 70.24%, respectively, as shown in Table S2 in the Supporting Information. The longer-lived PL decay time of $CsPbI_3$:Br:InI_3 film can be ascribed to the suppressed nonradiative recombination in perovskite films. Finally, we also used the method developed by Wrighton et al. to obtain the PL quantum yield (PLQY) for $CsPbI_3$, $CsPbI_3$:Br, and $CsPbI_3$:Br:InI_3 films, respectively.[45] Because of the weak PL intensities of $CsPbI_3$ and $CsPbI_3$:Br films, we cannot get their exact signals, which indicates the PLQYs for the two samples are too low. However, for the $CsPbI_3$:Br:InI_3 film, we calculated the PLQY to be 19%, which is much higher than the other two samples. This result further demonstrates the same conclusion with PL and TRPL curves (Figure 1e,f). In summary, compared with the $CsPbI_3$ film, the $CsPbI_3$:Br:InI_3 film possessed higher PL intensity, longer PL lifetime and higher PLQY, indicating that the introduction of Br^- and In^{3+} can significantly reduce the defect density and prolong the lifetime of charge carriers. Meanwhile, the $CsPbI_3$:Br:InI_3 film still maintains the same bandgap as the $CsPbI_3$ film.

It should also be emphasized that the new $CsPbI_3$:Br:InI_3 film has much higher humidity resistance than that of the $CsPbI_3$ film. **Figure 2**a shows that the $CsPbI_3$:Br:InI_3 film can be prepared successfully in >90% relative humidity atmosphere and its appearance is very uniform. While for the $CsPbI_3$ film, we must prepare it in the glovebox and its color will be changed to yellow immediately after we take it out of the glovebox (Table S1, Supporting Information). The transformation process of the $CsPbI_3$:Br:InI_3 film from the yellow phase to the black phase in high humidity air under 320 °C was displayed in Movie S1 in the Supporting Information.

To investigate the crystallinity of the $CsPbI_3$, $CsPbI_3$:Br, and $CsPbI_3$:Br:InI_3 films, X-ray diffraction (XRD) patterns were measured, as shown in Figure 2b. For the $CsPbI_3$ film, it is very unstable in air, therefore its XRD pattern is very ambiguous because of the large background. Since similar method were employed to prepare this film as reported in previous works and the peak at $2\theta = 13.5°$ being ascribed to the (001) plane of perovskite cubic phase, we indexed the $CsPbI_3$ perovskite as in cubic phase.[15] We plan to do more studies on this material and get much more stable $CsPbI_3$, such that its structure could be understood more thoroughly.[46–48] Figure S6 in the Supporting Information shows the standard XRD patterns of $CsPbI_3$ perovskite in cubic phase (PDF card NO. 04-016-2301). For the $CsPbI_3$:Br film, as expected, the incorporation of Br^- shrinks the cell and the peaks shift to the large angle direction, which is in accordance with previous work.[49] For the $CsPbI_3$:Br:InI_3 film, because the In^{3+} and I^- ions display the opposite effects on the unit cell, its peaks present a smaller shift and no new

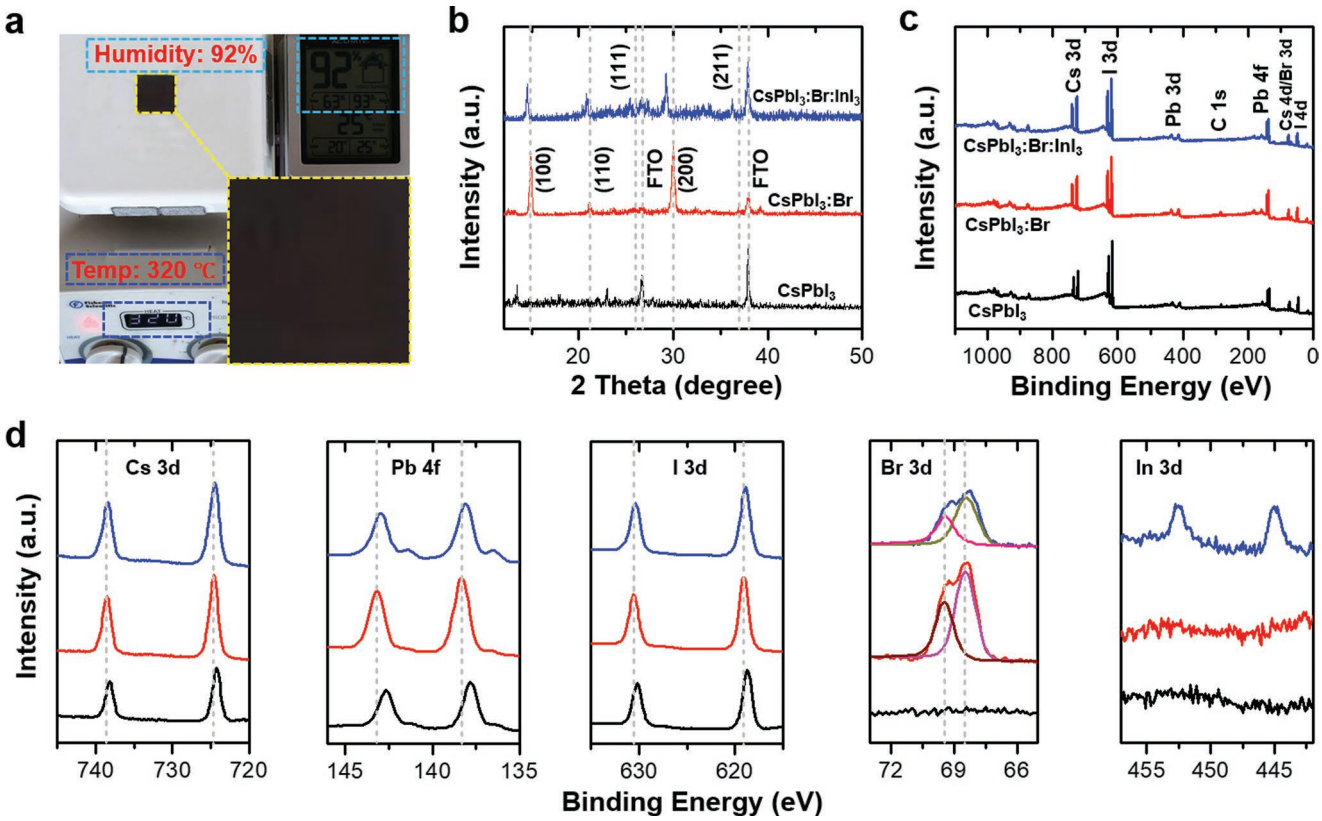

Figure 2. Structure and composition characterizations of $CsPbI_3$, $CsPbI_3$:Br, and $CsPbI_3$:Br:InI_3 films. a) Digital picture of $CsPbI_3$:Br:InI_3 films formed under 320 °C and 92% relative humidity atmosphere; b) XRD patterns and c) survey XPS spectra of $CsPbI_3$, $CsPbI_3$:Br, and $CsPbI_3$:Br:InI_3 films, respectively. Corresponding high-resolution XPS spectra of $CsPbI_3$, $CsPbI_3$:Br, and $CsPbI_3$:Br:InI_3 films at the d) Cs 3d, Pb 4f, I 3d, Br 3d, and In 3d regions, respectively.

phase can be found. However, regardless of the introduction of Br^- or InI_3, $CsPbI_3$:Br and $CsPbI_3$:Br:InI_3 films are still in perovskite cubic phase.[18]

To identify the composition of the $CsPbI_3$, $CsPbI_3$:Br, and $CsPbI_3$:Br:InI_3 films, X-ray photoelectron spectroscopy (XPS) analyses were carried out, as shown in Figure 2c. Because the peak position of Br 3d is very close to that of Cs 4d, it is very difficult to distinguish them in the survey XPS spectra. Moreover, the In peaks were not found in the $CsPbI_3$:Br:InI_3 film, which can be ascribed to a low atomic percentage and thus being out of the detection limits. Meanwhile, we also used the time-of-flight secondary ion mass spectrometry (TOF-SIMS) depth profile, a more sensitive method, to detect elemental distributions in the $CsPbI_3$:Br:InI_3 films, as shown in Figure S7 in the Supporting Information. First, TOF-SIMS depth profile indicates that In^{3+} ions were doped into the perovskite film successfully. Second, the TOF-SIMS depth profile reveals both In and Pb distributions with gradients showing a higher concentration of In and lower concentration of Pb on the surface, respectively. Non-uniform distribution of the In and Pb elements makes it very challenging to obtain the actual composition for this film. After calibration of C 1s peak to be 284.6 eV (Figure S8, Supporting Information), high-resolution XPS spectra at Cs 3d, Pb 4f, I 3d, Br 3d, and In 3d regions of the three kinds of films were measured, respectively, as shown in Figure 2d. These binding energies are listed in Table S3 in the Supporting Information. Figure 2d shows $CsPbI_3$:Br and $CsPbI_3$:Br:InI_3 films exhibit a characteristic peak at Br 3d region because of the incorporation of Br^- ions, and the $CsPbI_3$:Br:InI_3 film presents two In 3d peaks due to the introduction of InI_3, indicating that Br^- ions and In^{3+} ions were incorporated into the $CsPbI_3$ successfully. These results are also confirmed by the energy dispersive spectroscopy (EDS) spectrum and mapping, as shown in Figures S9 and S10 in the Supporting Information. Moreover, Figure 2d also reveals the shifts of peak positions in $CsPbI_3$:Br and $CsPbI_3$:Br:InI_3 films after Br^- and InI_3 being incorporated. These shifts can be ascribed to changes of chemical bonding caused by the incorporation of Br^- and In^{3+} ions, which is in accordance with the different lattice parameters observed in XRD patterns.

Subsequently, the $CsPbI_3$, $CsPbI_3$:Br, and $CsPbI_3$:Br:InI_3 films were employed to fabricate the all-inorganic PSCs as the absorber materials. **Figure 3**a shows the schematic view of all-inorganic PSCs with the structure of FTO/compact TiO_2 (c-TiO_2)/mesoporous TiO_2 (m-TiO_2)/inorganic perovskites/carbon. Clearly, all organic components that are expensive and/or lack of long-term stability in the traditional organic–inorganic PSCs were completely eliminated. Figure 3b reveals cross-sectional scanning electron microscopy (SEM) image of the all-inorganic PSCs based on $CsPbI_3$:Br:InI_3, which depicts a uniform deposition. The thickness of the $CsPbI_3$:Br:InI_3 is determined to be ≈350 nm. Figure 3c shows the energy band

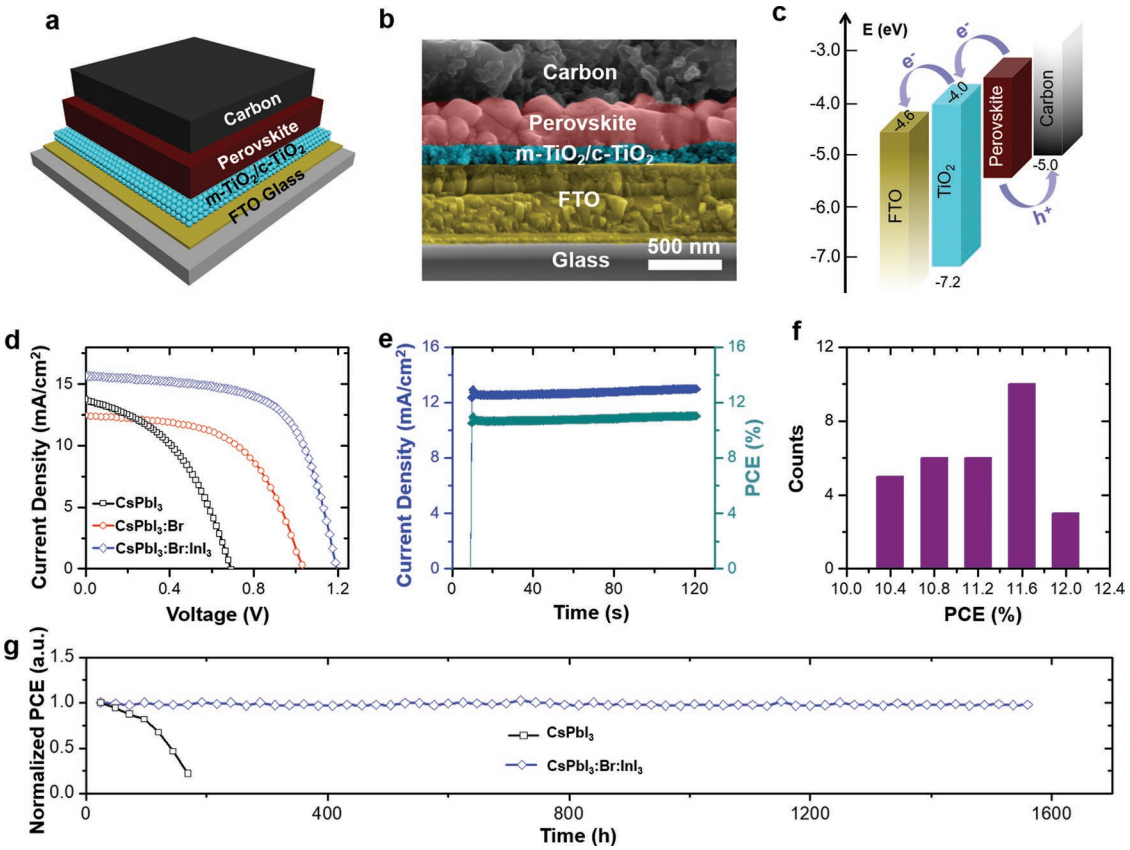

Figure 3. Photovoltaic performances of all-inorganic PSCs based on $CsPbI_3$, $CsPbI_3$:Br, and $CsPbI_3$:Br:InI_3 films. a) Schematic view and b) cross-sectional SEM image of all-inorganic PSCs with the structures of FTO/c-TiO_2/m-TiO_2/inorganic perovskites/carbon. c) Energy level diagram of all-inorganic PSCs. d) *J–V* plots of all-inorganic PSCs based on $CsPbI_3$, $CsPbI_3$:Br, and $CsPbI_3$:Br:InI_3 films, respectively. e) Current density and PCE as functions of time for the all-inorganic PSC based on $CsPbI_3$:Br:InI_3. f) Statistical histogram of the PCEs of 30 individual all-inorganic PSCs based on $CsPbI_3$:Br:InI_3. g) Normalized PCEs of all-inorganic PSCs based on $CsPbI_3$ and $CsPbI_3$:Br:InI_3 as a function of storage time in ambient atmosphere.

levels of all-inorganic PSCs, which reveal the electron extraction from the CBM of all-inorganic perovskites to that of the TiO_2 layer and the hole extraction from the VBM of all-inorganic perovskites to that of the carbon electrode smoothly.

Like previous halide-mixed perovskite, light-induced phase separation has likewise been found in this work (Figure S11, Supporting Information).[7,50–52] Therefore, before getting the *J–V* plots, light soaking process is needed for all PSCs. The photocurrent density–voltage (*J–V*) plots of the three kinds of all-inorganic PSCs are shown in Figure 3d, and the corresponding photovoltaic parameters are summarized in Table S1 in the Supporting Information. The all-inorganic PSC based on $CsPbI_3$ exhibits a PCE of 4.12%, which is comparable to the previous literature value without any treatment (Table S1, Supporting Information). Moreover, the all-inorganic PSC based on $CsPbI_3$ also gives an V_{OC} of 0.69 V, which is in accordance with the DFT calculations (Figure 1a,b). As expected, when Br^- ions were incorporated, the all-inorganic PSC based on $CsPbI_3$:Br presents higher V_{OC} of 1.03 V and fill factor (FF) of 0.56 because of the suppressed defect density by the incorporation of Br^-, and a lower current density (J_{SC}) of 12.46 mA cm^{-2} because of the increased bandgap, finally leading to a higher PCE of 7.22%. Moreover, when In^{3+} ions were further introduced, the all-inorganic PSC based on $CsPbI_3$:Br:InI_3 demonstrates an increase of all performance parameters. Specifically, the all-inorganic PSC based on $CsPbI_3$:Br:InI_3 shows the highest PCE of 12.04% with a J_{SC} of 15.68 mA cm^{-2}, a V_{oc} of 1.20 V, a FF of 0.64, respectively. As mentioned above, the best feed ratio of Pb:In for $CsPbI_3$:Br:InI_3 film is 85:15, because this perovskite shows the smallest bandgap (Figure S3, Supporting Information). Meanwhile, the photovoltaic performances of PSCs based on the perovskites with other ratios of Pb:In were also displayed, as shown in Figure S12 in the Supporting Information. A summary of photovoltaic performances of previous PSCs based on all-inorganic perovskites has been listed in Table S1 in the Supporting Information. Several PSCs displayed slightly higher PCEs than our PSC in this study; however, strictly speaking they were not all-inorganic PSCs because the organic hole transport materials (such as Spiro-MeOTAD or PTAA) were utilized in their structures. Moreover, most of them used noble metal as the counter electrodes, which increased the cost dramatically. Figure 3e reveals the plots of J_{SC} and PCE as functions of time for the all inorganic PSC based on $CsPbI_3$:Br:InI_3, indicating the J_{SC} and PCE is very stable under constant illumination. The *J–V* plots of the all-inorganic PSC based on $CsPbI_3$:Br:InI_3 were measured by the forward and reverse scan modes (Figure S13, Supporting Information), which reveal a minor hysteresis. To further confirm the reproducibility, 30 individual all-inorganic

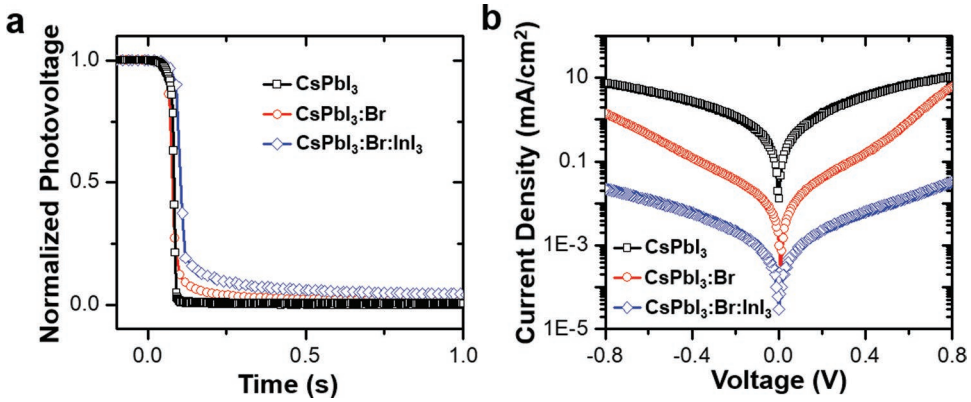

Figure 4. a) V_{OC} decay curves and b) dark J–V curves of the all-inorganic PSCs based on $CsPbI_3$, $CsPbI_3$:Br, and $CsPbI_3$:Br:InI_3 films.

PSCs based on $CsPbI_3$:Br:InI_3 were fabricated, as shown in Figure 3f. The statistical histogram shows that the PCE values of these 30 cells distribute over a narrow range with an average PCE of 11.24%, which can be ascribed to the highly repeatable preparation process of $CsPbI_3$:Br:InI_3 films with superior quality and homogenous thickness. The long-term stability of all-inorganic PSCs based on $CsPbI_3$:Br:InI_3 was also measured. Figure 3g and Figure S14 (Supporting Information) exhibit the time-dependent PCE, J_{SC}, V_{OC}, and FF retentions of encapsulated all-inorganic PSCs in air. Remarkably, the encapsulated PSC exhibited excellent stability, showing no degradation even after storage in ambient atmosphere for more than two months.

The high PCE of the all-inorganic PSC based on $CsPbI_3$:Br:InI_3 obtained in this study can be attributed to the relative small bandgap and low defect density. To quantitatively evaluate the defect density of these three kinds of films, we conducted transient V_{OC} decay under the open-circuit condition to understand the balanced charge-carrier transport in all-inorganic PSCs. **Figure 4**a shows the V_{OC} as a function of time starting from the illuminated steady-state equilibrium to the dark equilibrium. Among the three kinds of all-inorganic PSCs, the all-inorganic PSC based on $CsPbI_3$:Br:InI_3 film displays the lowest V_{OC} decay process, suggesting this film possesses the lowest recombination rate, and thus the lowest defect density. Moreover, the low defect density was also confirmed indirectly by the dark current measurement, as shown in Figure 4b. The dark current density of the all-inorganic PSC based on $CsPbI_3$:Br:InI_3 film is several orders of magnitude lower than the other two all-inorganic PSCs. This means that the defect density has been suppressed by introducing Br^- and In^{3+} ions, and a lower recombination rate was achieved.

In summary, a new all-inorganic perovskite material, $CsPbI_3$:Br:InI_3, was prepared using the facile solution-based method. By incorporating Br^- and In^{3+} in $CsPbI_3$, this new perovskite possessed the same bandgap as $CsPbI_3$, while significantly reduced the defect density. Moreover, the fabrication process of this new perovskite is very convenient and scalable, and it can be achieved under extremely high humidity atmosphere without the need of a glovebox. In this work, carbon film was used as the counter electrode for all-inorganic PSCs to avoid the high cost and the long-term instability in the traditional PSCs caused by noble metal electrodes and labile organic components. The all-inorganic PSCs based on $CsPbI_3$:Br:InI_3 exhibited the PCE and V_{OC} as high as 12.04% and 1.20 V, respectively. Additionally, the encapsulated all-inorganic PSCs revealed excellent stability in air for more than two months. The result shows that defect engineering is an effective approach for improving the performance of all-inorganic PSCs.

Supporting Information

Supporting Information is available from the Wiley Online Library or from the author.

Acknowledgements

J.L. and X.H. contributed to this work equally. This work was supported by the Peter M and Ruth L Nicholas Postdoctoral Fellowship in Nanotechnology (H21065) and the Welch Foundation grant C-1716. X.H. thanks the China Scholarship Council for partial support and Fundamental Research Funds for the Central Universities (3102019QD0418, 3102019ZD0402). ToF-SIMS analysis were carried out with support provided by the National Science Foundation CBET-1626418. This work conducted in part using resources of the Shared Equipment Authority at Rice University.

Conflict of Interest

The authors declare no conflict of interest.

Keywords

all-inorganic solar cells, $CsPbX_3$, defect engineering, indium, perovskite solar cells

Received: May 30, 2019
Revised: September 23, 2019
Published online: November 4, 2019

[1] J. Burschka, N. Pellet, S. J. Moon, R. Humphry-Baker, P. Gao, M. K. Nazeeruddin, M. Gratzel, *Nature* **2013**, *499*, 316.
[2] M. Z. Liu, M. B. Johnston, H. J. Snaith, *Nature* **2013**, *501*, 395.
[3] Q. F. Dong, Y. J. Fang, Y. C. Shao, P. Mulligan, J. Qiu, L. Cao, J. S. Huang, *Science* **2015**, *347*, 967.

[4] D. Shi, V. Adinolfi, R. Comin, M. J. Yuan, E. Alarousu, A. Buin, Y. Chen, S. Hoogland, A. Rothenberger, K. Katsiev, Y. Losovyj, X. Zhang, P. A. Dowben, O. F. Mohammed, E. H. Sargent, O. M. Bakr, *Science* **2015**, *347*, 519.
[5] S. D. Stranks, G. E. Eperon, G. Grancini, C. Menelaou, M. J. P. Alcocer, T. Leijtens, L. M. Herz, A. Petrozza, H. J. Snaith, *Science* **2013**, *342*, 341.
[6] N. J. Jeon, J. H. Noh, W. S. Yang, Y. C. Kim, S. Ryu, J. Seo, S. I. Seok, *Nature* **2015**, *517*, 476.
[7] A. Y. Mei, X. Li, L. F. Liu, Z. L. Ku, T. F. Liu, Y. G. Rong, M. Xu, M. Hu, J. Z. Chen, Y. Yang, M. Gratzel, H. W. Han, *Science* **2014**, *345*, 295.
[8] G. C. Xing, N. Mathews, S. Y. Sun, S. S. Lim, Y. M. Lam, M. Gratzel, S. Mhaisalkar, T. C. Sum, *Science* **2013**, *342*, 344.
[9] Y. Yang, J. B. You, *Nature* **2017**, *544*, 155.
[10] J. P. Correa-Baena, M. Saliba, T. Buonassisi, M. Gratzel, A. Abate, W. Tress, A. Hagfeldt, *Science* **2017**, *358*, 739.
[11] M. Saliba, T. Matsui, J. Y. Seo, K. Domanski, J. P. Correa-Baena, M. K. Nazeeruddin, S. M. Zakeeruddin, W. Tress, A. Abate, A. Hagfeldt, M. Gratzel, *Energy Environ. Sci.* **2016**, *9*, 1989.
[12] M. Saliba, T. Matsui, K. Domanski, J. Y. Seo, A. Ummadisingu, S. M. Zakeeruddin, J. P. Correa-Baena, W. R. Tress, A. Abate, A. Hagfeldt, M. Gratzel, *Science* **2016**, *354*, 206.
[13] J. Liang, C. X. Wang, Y. R. Wang, Z. R. Xu, Z. P. Lu, Y. Ma, H. F. Zhu, Y. Hu, C. C. Xiao, X. Yi, G. Y. Zhu, H. L. Lv, L. B. Ma, T. Chen, Z. X. Tie, Z. Jin, J. Liu, *J. Am. Chem. Soc.* **2016**, *138*, 15829.
[14] J. Liang, J. Liu, Z. Jin, *Sol. RRL* **2017**, *1*, 1700086.
[15] G. E. Eperon, G. M. Paterno, R. J. Sutton, A. Zampetti, A. A. Haghighirad, F. Cacialli, H. J. Snaith, *J. Mater. Chem. A* **2015**, *3*, 19688.
[16] A. Swarnkar, A. R. Marshall, E. M. Sanehira, B. D. Chernomordik, D. T. Moore, J. A. Christians, T. Chakrabarti, J. M. Luther, *Science* **2016**, *354*, 92.
[17] Q. S. Ma, S. J. Huang, X. M. Wen, M. A. Green, A. W. Y. Ho-Baillie, *Adv. Energy Mater.* **2016**, *6*, 1502202.
[18] R. J. Sutton, G. E. Eperon, L. Miranda, E. S. Parrott, B. A. Kamino, J. B. Patel, M. T. Horantner, M. B. Johnston, A. A. Haghighirad, D. T. Moore, H. J. Snaith, *Adv. Energy Mater.* **2016**, *6*, 1502458.
[19] S. Dastidar, D. A. Egger, L. Z. Tan, S. B. Cromer, A. D. Dillon, S. Liu, L. Kronik, A. M. Rappe, A. T. Fafarman, *Nano Lett.* **2016**, *16*, 3563.
[20] M. Kulbak, S. Gupta, N. Kedem, I. Levine, T. Bendikov, G. Hodes, D. Cahen, *J. Phys. Chem. Lett.* **2016**, *7*, 167.
[21] P. F. Luo, W. Xia, S. W. Zhou, L. Sun, J. G. Cheng, C. X. Xu, Y. W. Lu, *J. Phys. Chem. Lett.* **2016**, *7*, 3603.
[22] L. A. Frolova, D. V. Anokhin, A. A. Piryazev, S. Y. Luchkin, N. N. Dremova, K. J. Stevenson, P. A. Troshin, *J. Phys. Chem. Lett.* **2017**, *8*, 67.
[23] E. M. Hutter, R. J. Sutton, S. Chandrashekar, M. Abdi-Jalebi, S. D. Stranks, H. J. Snaith, T. J. Sayenije, *ACS Energy Lett.* **2017**, *2*, 1901.
[24] Y. G. Kim, T. Y. Kim, J. H. Oh, K. S. Choi, Y. J. Kim, S. Y. Kim, *Phys. Chem. Chem. Phys.* **2017**, *19*, 6257.
[25] J. Liang, C. X. Wang, P. Y. Zhao, Z. P. Lu, Y. Ma, Z. R. Xu, Y. R. Wang, H. F. Zhu, Y. Hu, G. Y. Zhu, L. B. Ma, T. Chen, Z. X. Tie, J. Liu, Z. Jin, *Nanoscale* **2017**, *9*, 11841.
[26] D. Y. Heo, S. M. Han, N. S. Woo, Y. J. Kim, T. Y. Kim, Z. T. Luo, S. Y. Kim, *J. Phys. Chem. C* **2018**, *122*, 15903.
[27] B. Li, Y. A. Zhang, L. Fu, T. Yu, S. J. Zhou, L. Y. Zhang, L. W. Yin, *Nat. Commun.* **2018**, *9*, 1076.
[28] S. S. Xiang, W. P. Li, Y. Wei, J. M. Liu, H. C. Liu, L. Q. Zhu, H. N. Chen, *Nanoscale* **2018**, *10*, 9996.
[29] Q. S. Zeng, X. Y. Zhang, X. L. Feng, S. Y. Lu, Z. L. Chen, X. Yong, S. A. T. Redfern, H. T. Wei, H. Y. Wang, H. Z. Shen, W. Zhang, W. T. Zheng, H. Zhang, J. S. Tse, B. Yang, *Adv. Mater.* **2018**, *30*, 1705393.
[30] L. X. Zhang, B. Li, J. F. Yuan, M. R. Wang, T. Shen, F. Huang, W. Wen, G. Z. Cao, J. J. Tian, *J. Phys. Chem. Lett.* **2018**, *9*, 3646.
[31] Y. Z. Jiang, J. Yuan, Y. X. Ni, J. Yang, Y. Wang, T. G. Jiu, M. J. Yuan, J. Chen, *Joule* **2018**, *2*, 1356.
[32] Q. Wang, X. P. Zheng, Y. H. Deng, J. J. Zhao, Z. L. Chen, J. S. Huang, *Joule* **2017**, *1*, 371.
[33] B. Y. Zhao, S. F. Jin, S. Huang, N. Liu, J. Y. Ma, D. J. Xue, Q. W. Han, J. Ding, Q. Q. Ge, Y. Q. Feng, J. S. Hu, *J. Am. Chem. Soc.* **2018**, *140*, 11716.
[34] J. Tian, Q. Xue, X. Tang, Y. Chen, N. Li, Z. Hu, T. Shi, X. Wang, F. Huang, C. Brabec, H. Yip, Y. Cao, *Adv. Mater.* **2019**, *31*, 1901152.
[35] Y. Wang, M. Dar, L. K. Ono, T. Zhang, M. Kan, Y. Li, L. Zhang, X. Wang, Y. Yang, X. Gao, Y. Qi, M. Grätzel, Y. Zhao, *Science* **2019**, *365*, 591.
[36] W. S. Subhani, K. Wang, M. Du, X. Wang, S. Liu, *Adv. Energy Mater.* **2019**, *9*, 1803785.
[37] H. Wang, H. Bian, Z. Jin, L. Liang, D. Bai, Q. Wang, S. Liu, *Sol. RRL* **2018**, *2*, 1800216.
[38] Y. Li, J. Duan, H. Yuan, Y. Zhao, B. He, Q. Tang, *Sol. RRL* **2018**, *2*, 1800164.
[39] B. G. Choi, J. H. Kim, D. H. Kim, K. S. Lee, T. S. Lee, B. Cheong, Y. J. Baik, W. M. Kim, *J. Eur. Ceram. Soc.* **2005**, *25*, 2161.
[40] P. K. Nayak, M. Sendner, B. Wenger, Z. Wang, K. Sharma, A. J. Ramadan, R. Lovrincic, A. Pucci, P. K. Madhu, *J. Am. Chem. Soc.* **2018**, *140*, 574.
[41] A. L. Abdelhady, M. I. Saidaminov, B. Murali, V. Adinolfi, O. Voznyy, K. Katsiev, E. Alarousu, R. Comin, I. Dursun, L. Sinatra, E. H. Sargent, O. F. Mohammed, O. M. Bakr, *J. Phys. Chem. Lett.* **2016**, *7*, 295.
[42] Y. Hu, F. Bai, X. Liu, Q. Ji, X. Miao, T. Qiu, S. Zhang, *ACS Energy Lett.* **2017**, *2*, 2219.
[43] C. Wang, C. Zhang, S. Wang, G. Liu, H. Xia, S. Tong, J. He, D. Niu, C. Zhou, K. Ding, Y. Gao, J. Yang, *Sol. RRL* **2018**, *2*, 1700209.
[44] J. S. Yeo, R. Kang, S. Lee, Y. J. Jeon, N. Myoung, C. L. Lee, D. Y. Kim, J. M. Yun, Y. H. Seo, S. S. Kim, S. I. Na, *Nano Energy* **2015**, *12*, 96.
[45] M. S. Wrighton, D. S. Ginley, D. L. Morse, *J. Phys. Chem.* **1974**, *78*, 2229.
[46] B. Zhao, S. Jin, S. Huang, N. Liu, J. Ma, D. Xue, Q. Han, J. Ding, Q. Ge, Y. Feng, J. Hu, *J. Am. Chem. Soc.* **2018**, *140*, 11716.
[47] R. J. Sutton, M. R. Filip, A. A. Haghighirad, N. Sakai, B. Wenger, F. Giustino, H. J. Snaith, *ACS Energy Lett.* **2018**, *3*, 1787.
[48] H. Chen, S. Xiang, W. Li, H. Liiu, L. Zhu, S. Yang, *Sol. RRL* **2018**, *2*, 1700188.
[49] R. E. Beal, D. J. Slotcavage, T. Leijtens, A. R. Bowring, R. A. Belisle, W. H. Nguyen, G. F. Burkhard, E. T. Hoke, M. D. McGehee, *J. Phys. Chem. Lett.* **2016**, *7*, 746.
[50] J. S. Nieagoda, B. J. Foley, A. Z. Chen, J. J. Choi, *ACS Energy Lett.* **2017**, *2*, 1043.
[51] E. Rezaee, X. Liu, Q. Hu, L. Dong, Q. Chen, J. Pan, Z. Xu, *Sol. RRL* **2018**, *2*, 1800200.
[52] E. T. Hoke, D. J. Slotcavage, E. R. Dohner, A. R. Bowring, H. I. Karunadasa, M. D. McGehee, *Chem. Sci.* **2015**, *6*, 613.